Chemical Engineering Journal 435 (2022) 134733

Contents lists available at ScienceDirect

Chemical Engineering Journal

journal homepage: www.elsevier.com/locate/cej

Systematic calibration of N_2O emissions from a full-scale WWTP including a tracer test and a global sensitivity approach

Borja Solís [a], Albert Guisasola [a,*], Maite Pijuan [b,c], Lluís Corominas [b,c], Juan Antonio Baeza [a]

[a] GENOCOV. Departament d'Enginyeria Química, Biològica i Ambiental. Escola d'Enginyeria. Universitat Autònoma de Barcelona, 08193, Bellaterra (Barcelona), Spain
[b] Catalan Institute for Water Research (ICRA), Scientific and Technological Park of the University of Girona, Emili Grahit 101, 17003, Girona, Spain
[c] Universitat de Girona, Plaça de Sant Domènec 3, 17004 Girona, Spain

ARTICLE INFO

Keywords:
Nitrous oxide
WWTP modelling
Global sensitivity analysis
Dynamic calibration

ABSTRACT

Nitrous oxide (N_2O) is a greenhouse gas (GHG) emitted during biological nitrogen removal from wastewater treatment plants (WWTPs). Some modelling tools have been proposed to predict N_2O emissions during the design and operation of WWTPs. In this study, the novel ASM2d-N_2O model, which accounts for the production of N_2O in nutrient removal WWTPs, was used to study the associated emissions from a full-scale WWTP with two independent lines. Firstly, the hydraulics of the WWTP was characterized by a residence time distribution test, showing the flow was equally divided into the two treatment lines (49.3 vs. 50.7%), that each reactor worked as an ideal continuous stirred tank reactor and the secondary settler model flux was similar to a plug-flow reactor. The ASM2d-N_2O model was then calibrated using experimental data obtained under dynamic conditions. A global sensitivity analysis was used to select, among 59 model parameters, five candidates that resulted to be related to nitrifying organisms. Different parameter subsets up to four parameters were evaluated, being the subset [μ_{NOB}, q_{AOB_AMO}, K_{O2_NOB}, K_{NO2_NOB}] the best, achieving 53.3% reduction of the calibration cost function. The model fit obtained provided a reasonably description of nutrients and N_2O emission trends, considering the inherent operational variability suffered in full-scale WWTPs. Finally, a simulation-based study showed that, for the given WWTP and operational conditions, an unbalanced distribution of flow-rate between the two treatment lines did not result in a significant increase on N_2O emissions. The results obtained show that this model can be a suitable tool for predicting N_2O emissions in full-scale WWTPs, and can therefore be used to find operational conditions that help to minimise these emissions.

Abbreviations: AER, Aerobic reactor; ANA, Anaerobic reactor; ANX, Anoxic reactor; AOB, Ammonia Oxidizing Bacteria; AS, Activated Sludge; ASM, Activated Sludge Model; ASM2, Activated Sludge Model number 2; ASMN, Activated Sludge Model for Nitrogen; BNR, Biological Nitrogen Removal; Br^-, Bromide; C, Carbon; CCF, Calibration Cost Function; CCF_{N2O}, Calibration Cost Function for Nitrous oxide; CCF_{NH4}, Calibration Cost Function for Ammonium; CCF_{NO2}, Calibration Cost Function for Nitrite; CCF_{NO3}, Calibration Cost Function for Nitrate; CritD, FIM D criteria; CritModE, FIM modified E criteria; COD, Chemical Oxygen Demand; COD_{fil}, Filtered COD; $COD_{fil,\ eff}$, Effluent filtered COD; COD_{sol}, Soluble COD; COD_{tot}, Total COD; CSTR, Continuous Stirred Tank Reactor; DO, Dissolved Oxygen; FIM, Fisher Information Matrix; GHG, Greenhouse gas; GSA, Global Sensitivity Analysis; GWP, Global Warming Potential; HCCF, Hydraulic Calibration Cost Function; HD pathway, Heterotrophic Denitrification pathway; IR, Internal Recirculation; IWA, International Water Association; KBr, Potassium Bromide; MAE, Mean Absolute Error; MC, Monte Carlo; N, Nitrogen; N_2, Nitrogen gas; N_2O, Nitrous oxide; N_2O-EF, Nitrous oxide emission factor; N_2O-N, Nitrous oxide nitrogen; ND pathway, Nitrifier Denitrification pathway; NH_2OH, Hydroxylamine; NH_4^+, Ammonium; NN pathway, Nitrifier Nitrification pathway; NO, Nitric oxide; NO_2^-, Nitrite; NO_3^-, Nitrate; NOB, Nitrite Oxidizing Bacteria; NormD, FIM normalized D criteria; P, Phosphorus; PAO, Polyphosphate Accumulating Organisms; PCCF, Preliminary Calibration Cost Function; PO_4^{3-}, Phosphate; R^2, Coefficient of determination; RDE, FIM ratio between NormD and CritModE; RMSE, Root Mean Square Error; RSA, Regional Sensitivity Analysis; RTD, Residence Time Distribution; SI, Supplementary Information; S_i, Sensitivity index; SS, Steady-State; TKN, Total Kjeldahl Nitrogen; WWTP, Wastewater Treatment Plant; X_{MeOH}, Ferric Hydroxide state variable.

* Corresponding author.
E-mail addresses: Borja.solis@uab.cat (B. Solís), albert.guisasola@uab.cat (A. Guisasola), mpijuan@icra.cat (M. Pijuan), lcorominas@icra.cat (L. Corominas), JuanAntonio.Baeza@uab.cat (J.A. Baeza).

https://doi.org/10.1016/j.cej.2022.134733
Received 28 May 2021; Received in revised form 26 December 2021; Accepted 12 January 2022
Available online 18 January 2022

1. Introduction

Over the past years, concerns regarding the sustainability of wastewater treatment plants (WWTPs) have increased, with particular emphasis on the carbon (C) footprint. Nitrous oxide (N_2O) is a greenhouse gas (GHG) that is emitted during biological nitrogen removal (BNR) in WWTPs. Due to its high global warming potential, 265 times higher than that of carbon dioxide (CO_2) [1], the C footprint of WWTPs are highly sensitive to N_2O emissions [2]. In addition, N_2O is an ozone layer depletion gas [3]. Measurement campaigns on full scale WWTPs have shown high variability on the measured N_2O emissions, with a N_2O emission factor (N_2O-EF, defined as the fraction of influent nitrogen load emitted as N_2O) ranging between 0.01% and 1.8%, and in some cases even higher than 10% [4–6].

The biological pathways for N_2O production during BNR are related to nitrification and denitrification processes [4], being the first one the major contributor to N_2O emissions in full–scale plants. Nitrification consists of two coupled processes: i) ammonium (NH_4^+) oxidation to hydroxylamine (NH_2OH), nitric oxide (NO) and nitrite (NO_2^-) by ammonia oxidizing bacteria (AOB) [7] through the nitritation process and ii) nitrite (NO_2^-) oxidation to nitrate (NO_3^-) by nitrite oxidizing bacteria (NOB) through the nitratation process. AOB are responsible of N_2O production during BNR by two possible pathways. On the one hand, N_2O can be produced through the biological NO reduction due to incomplete NH_2OH oxidation: the NH_2OH incomplete oxidation pathway (NN pathway) [4]. On the other hand, AOB can produce N_2O by the sequential reduction of NO_2^- to NO and N_2O: the nitrifier denitrification pathway (ND pathway). There exists a third biological N_2O production pathway during the denitrification process (HD pathway). N_2O is formed as an obligate intermediate of the four step reduction reactions of NO_3^- to NO_2^- and then to NO, N_2O and finally dinitrogen gas (N_2) [4,8,9].

Mathematical models have been widely applied to the prediction of nitrogen (N) and phosphorus (P) removal in WWTPs since the development of the activated sludge models (ASM) by the International Water Association (IWA) [10]. Over the past years, modelling BNR has gained more attention in view of a better understanding of N_2O production, accumulation and emission. The ability to predict N_2O emissions serves as a method for verifying hypothesis related to fundamental mechanisms for N_2O production, and it can be used to anticipate N_2O emissions in the design and operation of WWTPs, as well as in the design of potential mitigation strategies [6,11,12].

Different models have been developed aiming at predicting lab-scale or full-scale N_2O emissions [6,12–16]. These models are based on different assumptions, incorporating one, two or three of the biological pathways for N_2O production (ND, NN or HD). Regarding nitrification, it was seen that the models only including a single N_2O production pathway could not explain all the experimental data in the literature. Therefore, it was formulated that both NN and ND can occur at the same time depending on the operating conditions [14]. Among the different published N_2O models, the ASM2d-N_2O model developed by Massara et al. [16] is an ASM type model that: includes N, P and organic matter removal; integrates all the microbial pathways for N_2O production and consumption; contains N_2O stripping modelling and estimates the N_2O-EF under a wide range of operating conditions. Therefore, the ASM2d-N_2O model is a promising tool for developing N_2O mitigation strategies during full-scale WWTP. However, although the different sub-models of the whole ASM2d-N_2O were calibrated separately, the prediction capability of the ASM2d-N_2O model has not been proved during full-scale treatment.

With regard to the modelling of full-scale WWTPs, the variability of the operational parameters or the hydraulic conditions of the reactor itself is often not considered, and simplifications of ideality end up being used, modelling the reactors as continuous stirred tank reactor (CSTR) with perfectly known inlet and outlet flow rates. However, hydraulics should be considered to obtain more realistic model predictions. Hydraulics is considered relevant from two perspectives that affect the performance of the plant: pollutant degradation depends on the flow rate and the control of the process is based on concentrations measured in specific points in the reactor [17]. Classical tools as residence time distribution (RTD) techniques with tracer experiments have been applied to investigate the behaviour of full-scale WWTPs, in order to detect hydraulic problems such as plug-flow behaviour [18], unoptimized inlet flow distribution ratio [19], short-circuiting flows and dead zones [20,21]. Studies in full-scale WWTPs have demonstrated that these hydrodynamic anomalies can reduce pollutant removal and increase management costs [21]. Moreover, biased sampling strategies not considering hydraulic RTD and daily flow variations and concentrations can also lead to erroneous conclusions [22]. In the present study, where the plant consists of two parallel lines, there was concern about the possible effect on N_2O emissions if there was an imbalance between the flows treated in both lines. Plant overloading or changes in plant load have been one of the operating conditions believed to have a significant impact on N_2O emissions [16], and hence, a maldistribution of flow rates between the lines could cause an overloaded line significantly increasing its N_2O emissions.

Therefore, the main objective of this study was to comprehensively calibrate the ASM2d-N_2O model using dynamic data from a full-scale municipal WWTP. Firstly, an RTD experiment was performed to calibrate WWTP hydraulics, as an essential initial step to obtain accurate predictions of the N-species and N_2O emissions. Then, an experimental campaign was carried out during three days in different zones of the WWTP to capture its N_2O emission dynamics. The parameter subset selection to calibrate the ASM2d-N_2O model was obtained through a global sensitivity analysis (GSA) method, to capture the interactions between the parameters and to select the parameter subset independently from the initial parameter value. The identifiability of the parameter subsets was evaluated using the Fisher information matrix (FIM) methodology. Finally, a simulation-based study was carried out to assess the possible effect that an incorrect flow distribution between treatment lines had on the N_2O emissions from the WWTP due to possible treatment line overloading and changes in treatment plant loads.

2. Materials and methods

2.1. Girona WWTP description

The full-scale urban WWTP is located in Girona (Catalonia, Spain) with a design capacity of 206250 population equivalent and 55000 m^3 d^{-1}. A schematic overview of the WWTP process layout is shown in Fig. 1. After the pre-treatment (grit and gross removal), the influent is distributed in three rectangular lamella-plate primary clarifiers. The biological section has a 5-stage Bardenpho configuration. It consists of two main treatment lines with seven separated reactors in each line. The wastewater flows through an anaerobic reactor (ANA1, 1335 m^3), an anoxic reactor (ANX1, 4554 m^3), three aerobic reactors with the same volume (AER1 to AER3, 1929 m^3), a second anoxic reactor (ANX2, 1276 m^3) and finally a fourth aerobic reactor (AER4, 1409 m^3). The internal recycle (IR) flows from the third aerobic reactor (AER3) to the first anoxic reactor (ANX1) and it is independent in each line (Fig. 1). In addition, sodium aluminate is injected into each IR stream to favour chemical P precipitation. The flow is mixed again at the outlet of the last aerobic zone and divided into three parallel secondary clarifiers (5332 m^3 each settler) where the biomass is separated from the treated effluent. The concentrated outflows from each secondary clarifier are mixed and, after extracting the purge flow, recycled to the influent of the biological reactors. Aeration is supplied by blowers in the aerobic zones. Each line has a blower whose air is sparged through diffusers.

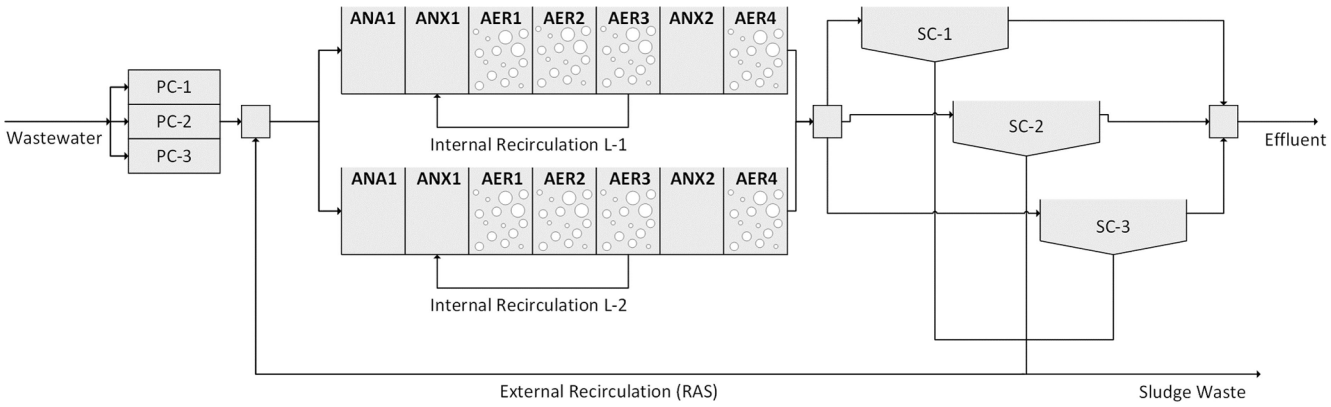

Fig. 1. Plant layout of the Girona WWTP (PC = Primary Clarifier, SC = Secondary Clarifier, ANA = Anaerobic reactor, ANX = Anoxic reactor and AER = Aerobic reactor.

2.2. Hydraulic characterization procedure

Tracer experiments to characterize the hydraulics of the secondary treatment of the WWTP (i.e. biological reactors and secondary clarifiers) were carried out with potassium bromide (KBr). The objectives of the hydraulic characterization were: 1) to determine the flow distribution between both treatment lines in the biological reactor, as the plant operators suspected that it was not equally distributed in each treatment line and 2) to understand the hydraulics of each reactor to identify possible dead-zones. An amount of 24.9 kg of KBr (16.7 kg of Br^-) was added to the influent of the primary clarifiers. During the experiment, samples were taken from different zones of the two treatment lines of the biological reactor and in the effluent. The locations of the tracer pulse and the different tracer samples zones are indicated in Figure S1 in section S1 of the Supplementary Information (SI).

The model structure used to determine the RTD of the activated sludge (AS) system of the Girona WWTP was the n-tanks in series [23], a widely used method in the calibration of full-scale WWTPs [18,24,25]. The pulse was added in the influent of the primary clarifiers but, for simulation purposes, the data at the effluent of the primary clarifiers were used as the input simulation because modelling of the complex hydraulic lamella-plates clarifiers of the primary settler was out of the scope of this work and was not needed for the WWTP calibration. As an initial approach, each vessel was considered to be an ideal CSTR and the influent flow was equally divided into each treatment line. Hence, each line of the secondary treatment was initially simulated as 8 tanks in series (7 reactors plus the secondary settler also simulated as a single tank). The mass balance of the tracer concentration in each tank is described by Equation (1):

$$V_i \cdot \frac{dC_i}{dt} = Q_i \cdot (C_{in,i} - C_i) \quad (1)$$

Where: V_i is the volume of reactor "i"; Q_i is the volumetric flowrate in reactor "i", $C_{in,i}$ is the inlet tracer concentration and C_i the tracer concentration in reactor "i".

The calibration cost function of the hydraulic experiment to be minimized was named HCCF (Equation (2)):

$$HCCF = \sum_{i=1}^{N} \frac{\max|C_{ANA1-L1}|}{\max|C_i|} \cdot \sqrt{(C_{i,exp} - C_{i,model})^2} \quad (2)$$

Where: "i" refers to each reactor; $C_{i,exp}$ is the experimental concentration; $C_{i,model}$ is the model prediction and $\max|C_{ANA1-L1}|/\max|C_i|$ is a weight factor to normalize the concentrations of each reactor to those of ANA1 from the biological treatment line one. Thus, each of the experimental inputs has the same influence on the HCCF.

2.3. Experimental data campaign

A three-day data sampling campaign was carried out from 18 to 20 July 2017 to calibrate the ASM2d-N_2O model at the Girona WWTP under dynamic conditions. Figure S1 in the supplementary information (SI) shows a scheme of the WWTP with the locations and data collected during the experimental data campaign. Only one biological treatment line was sampled (Line 1, Fig. 1). The data collected are summarized below:

- *Chemical analysis*: Grab samples were collected to analyse NH_4^+, NO_2^-, NO_3^- and PO_4^{3-} by ion chromatography (ICS5000, DIONEX) at different locations and intervals. The rationale of the sampling frequency was to be able to relate N_2O emissions to N-species. Therefore, the sampling frequency was increased in the reactors were N_2O emissions were monitored. Grab samples were taken 5 times a day at 3 h intervals (from 9:00 to 18:00) plus midnight for 3 days at reactors ANX1, AER1, AER3 and AER4. At reactors ANA1 and ANX2, the grab samples were taken less frequently, only 3 times a day. In addition, two refrigerated automatic samplers also took samples every 3 h during the 3 days of the data campaign (8 times per day) at the influent of the biological reactors and in AER2 reactor. Br^- was measured using a Dionex DX-500 ion chromatograph (Dionex Corp., Sunnyvale, CA, USA). The method detection limit (MDL) was 0.045 μg/l for Br^-. The practical limit of quantification (LOQ = 5 MDL) was 0.23 mg/l for Br^-.
- *Online sensors*: NH_4^+, COD, pH and temperature at the bioreactor inlet were continuously monitored utilizing two on-line ion-selective electrodes (ammo::lyser™) coupled to a monitoring station (S::CAN Messtechnik GmbH, Austria). In addition, three Dissolved Oxygen (DO) probes (oxi::lyser™) were installed in AER1, AER2 and AER3 coupled to the same S::CAN monitoring station.
- *Gas emission measurements*: N_2O emissions were measured in reactors AER1, AER2 and AER3 using a system with three gas collection hoods. The gas collected in the hoods was coupled with a monitoring unit to log gas temperature, pressure and flowrate. Part of the gas was pumped to a conditioning unit (M&C Tech group) to remove humidity and particles and finally the gas was conducted to an online analyser (Horiba VA3000). N_2O concentration (in ppmv), pressure, gas flowrate and temperature were logged at 15 s intervals. The analyser measured only one hood at a time in 20-minute intervals between each reactor. A detailed methodology for the gas emission measurement system can be found in Ribera-Guardia et al. [26].
- *Data from the WWTP SCADA system*: data of the hydraulics (biological influent, internal and external recirculation and wastage flowrates) and DO of the aerobic reactors were collected from the SCADA system of the WWTP.

Table 1
Symbols, description, default values at 20 °C, units and variation range of the ASM2d–N_2O parameters included in the GSA.

Parameter	Description	Default value at 20 °C	Units	Min/max range
K_H	Hydrolysis rate constant	3	d^{-1}	1.5 / 4.5
K_{O2_H}	Saturation/inhibition coefficient for O_2	0.2	g O_2 m^{-3}	0.1 / 0.3
K_{x_H}	Saturation coefficient for particulate COD	0.1	g X_S (g X_H) $^{-1}$	0.05 / 0.15
n_{NO3_H}	Anoxic hydrolysis reduction factor	0.6	–	0.3 / 0.9
n_{NO2_H}	Anoxic hydrolysis reduction factor	0.6	–	0.3 / 0.9
K_{NO3_H}	Saturation/inhibition coefficient for NO_3^-	0.5	g N m^{-3}	0.25 / 0.75
K_{NO2_H}	Saturation/inhibition coefficient for NO_2^-	0.5	g N m^{-3}	0.25 / 0.75
n_{fe_H}	Anaerobic hydrolysis reduction factor	0.4	–	0.2 / 0.6
μ_H	Maximum growth rate on substrate	6	g X_S (g X_H) $^{-1}d^{-1}$	3 / 9
K_{O2}	Saturation/inhibition coefficient for O_2	0.1	g O_2 m^{-3}	0.05 / 0.15
K_F	Saturation coefficient for growth on S_F	20	g COD m^{-3}	10 / 30
K_{NH4}	Saturation coefficient for NH_4^+ (nutrient)	0.05	g N m^{-3}	0.025 / 0.075
K_P	Saturation coefficient for PO_4^{3-} (nutrient)	0.01	g P m^{-3}	0.005 / 0.015
K_{ALK}	Saturation coefficient for alkalinity (HCO_3^-)	0.1	mole HCO_3^- m^{-3}	0.05 / 0.15
K_A	Saturation coefficient for growth on acetate S_A	20	g COD m^{-3}	10 / 30
K_{NO3}	Saturation/inhibition coefficient for NO_3^-	0.5	g N m^{-3}	0.25 / 0.75
K_{NO2}	Saturation/inhibition coefficient for NO_2^-	0.5	g N m^{-3}	0.25 / 0.75
n_{NO3_D}	Reduction factor for denitrification	0.28	–	0.14 / 0.42
q_{fe}	Maximum rate for fermentation	3	g S_F (g X_H) $^{-1}d^{-1}$	1.5 / 4.5
K_{fe_H}	Saturation coefficient for fermentation of S_F	4	g COD m^{-3}	2 / 6
b_H	Rate constant for lysis and decay	0.4	d^{-1}	0.2 / 0.6
n_{G3}	Anoxic growth factor (NO_2^-→NO)	0.16	–	0.08 / 0.24
n_{G4}	Anoxic growth factor (NO → N_2O)	0.35	–	0.175 / 0.525
n_{G5}	Anoxic growth factor (N_2O → N_2)	0.35	–	0.175 / 0.525
K_{S3}	Half-saturation coefficient for substrate	20	g COD m^{-3}	10 / 30
K_{S4}	Half-saturation coefficient for substrate	20	g COD m^{-3}	10 / 30
K_{S5}	Half-saturation coefficient for substrate	40	g COD m^{-3}	20 / 60
K_{NO2_Den}	Half-saturation coefficient for NO_2^-	0.2	g N m^{-3}	0.1 / 0.3
K_{OH4}	Half-saturation coefficient for O_2	0.1	g O_2 m^{-3}	0.05 / 0.15
K_{N2O_Den}	Half-saturation coefficient for N_2O	0.05	g N m^{-3}	0.025 / 0.075
K_{OH3}	Half-saturation coefficient for O_2	0.1	g O_2 m^{-3}	0.05 / 0.15
K_{NO_Den}	Half-saturation coefficient for NO	0.05	g N m^{-3}	0.025 / 0.075
K_{OH5}	Half-saturation coefficient for O_2	0.1	g O_2 m^{-3}	0.05 / 0.15
K_{I3NO}	NO inhibition coefficient (NO_2^-→NO)	0.5	g N m^{-3}	0.25 / 0.75
K_{I4NO}	NO inhibition coefficient (NO → N_2O)	0.3	g N m^{-3}	0.15 / 0.45
K_{I5NO}	NO inhibition coefficient (N_2O → N_2)	0.075	g N m^{-3}	0.038 / 0.112
μ_{AOB_HAO}	Maximum AOB growth rate	0.78	d^{-1}	0.39 / 1.17
q_{AOB_AMO}	Maximum rate for the AMO reaction	5.2	g N (g COD) $^{-1}$ d^1	2.6 / 7.8
K_{O2_AOB1}	AOB affinity constant for O_2 (AMO reaction)	1	g O^2 m^{-3}	0.5 / 1.5
K_{NH4_AOB}	AOB affinity constant for NH_4^+	0.2	g N m^{-3}	0.1 / 0.3
K_{O2_AOB2}	AOB affinity constant for O_2 (HAO reaction)	0.6	g O_2 m^{-3}	0.3 / 0.9
K_{NH2OH_AOB}	AOB affinity constant for NH_2OH	0.3	g N m^{-3}	0.15 / 0.45
q_{AOB_HAO}	Maximum rate for HAO reaction	5.2	g N (g COD) $^{-1}$ d^{-1}	2.6 / 7.8
$K_{NO\_AOB\_HAO}$	AOB affinity constant for NO (from HAO)	0.0003	g N m^{-3}	0.00015 / 0.00045
$q_{AOB\_N2O\_NN}$	Maximum N_2O production rate by NN pathway	0.0078	g N (g COD) $^{-1}$ d^{-1}	0.004 / 0.012
$K_{NO\_AOB\_NN}$	AOB affinity constant for NO (from NirK)	0.008	g N m^{-3}	0.004 / 0.012
$K_{O2\_AOB\_ND}$	AOB constant for O_2 effect on the ND pathway	0.5	g O^2 m^{-3}	0.25 / 0.75
$K_{I\_O2\_AOB}$	N_2O constant for production inhibition by O_2	0.8	g O^2 m^{-3}	0.4 / 1.2
K_{HNO2_AOB}	AOB affinity constant for HNO_2	0.004	g N m^{-3}	0.002 / 0.006
$q_{AOB\_N2O\_ND}$	Maximum N_2O production rate by the ND pathway	1.3	g N (g COD) $^{-1}$ d^{-1}	0.65 / 1.95
K_{ALK_AOB}	Saturation coefficient for alkalinity (HCO_3^-)	0.1	mole HCO_3^- m^{-3}	0.05 / 0.15
K_{P_AOB}	Saturation coefficient for PO_4^{3-} (nutrient)	0.01	g P m^{-3}	0.005 / 0.015
μ_{NOB}	Maximum NOB growth rate	0.78	d^{-1}	0.39 / 1.17
K_{O2_NOB}	Half-saturation coefficient for O_2	1.2	g O_2 m^{-3}	0.6 / 1.8
K_{ALK_NOB}	Saturation coefficient for alkalinity (HCO_3^-)	0.1	mole HCO_3^- m^{-3}	0.05 / 0.15
K_{NO2_NOB}	Saturation coefficient for NO_2^-	0.5	g N m^{-3}	0.25 / 0.75
K_{P_NOB}	Saturation coefficient for PO_4^{3-} (nutrient)	0.01	g P m^{-3}	0.005 / 0.015
b_{AOB}	Decay rate of AOB	0.096	d^{-1}	0.048 / 0.144
b_{NOB}	Decay rate of NOB	0.096	d^{-1}	0.048 / 0.144

2.4. *ASM2d-N_2O structure*

The ASM2d-N_2O kinetic model [16] was calibrated to describe the Girona WWTP. The ASM2d-N_2O model is able to predict COD, N and P removal and N_2O production. The model structure is based on the ASM2d model developed by Henze et al. [10], and extended to account for N_2O production with the 2–pathway model for N_2O emissions by AOB, developed by Pocquet et al. [14] and the denitrification processes with the activated sludge model for nitrogen (ASMN) developed by Hiatt and Grady [27]. The temperature dependence of the biological reactions was implemented following the guidelines of the activated sludge model No. 2 (ASM2) [10] to describe the different seasonal patterns. The subset of all parameters involved in ASM2d-N_2O, with calibrated parameters, stoichiometric matrix and kinetics rates can be found in section S9 of the SI. In addition, proportional controllers were modelled in each aerobic reactor to maintain the DO concentration at the measured DO in the WWTP. The manipulated variable of each proportional controller was the mass transfer coefficient for oxygen (k_La_{O2}) in each aerobic reactor.

2.5. *Global sensitivity analysis (GSA)*

A GSA was performed to identify the input factors (i.e. parameters) that most affected the model outputs and, therefore, the parameters that should be calibrated preferentially. The selected model output was the

calibration cost function (CCF), which is the sum of the squared differences between experimental data and dynamic model output (see section 2.6).

Among the different GSA methods, the Monte Carlo (MC) filtering or regional sensitivity analysis (RSA) was a suitable method to select the parameters that were not only more sensitive to CCF but also reduced it [28,29]. RSA is based on mapping the input factors space according to whether the associated output, i.e. the CCF, is below (i.e. "behavioural" samples) or above (i.e. "non-behavioural" samples) a predefined threshold [30,31]. The workflow used to apply the RSA method was [29]: 1) a range was defined for the input factor space and a MC experiment was performed. 2) The model outputs were classified as behavioural (B) or non-behavioural ($\overline{B}$) according to the specified threshold of the CCF and associated to the input factors values. 3) A set of binary elements was defined, distinguishing between two subsets for each parameter (X_i): the behavioural subset ($X_i|B$) and the non-behavioural subset ($X_i|\overline{B}$). 4) The Smirnov test (equation (3)) was performed for each input factor and used as a measure of the Sensitivity index (S_i) [29]; The parameters were ranked in order of influential on CCF reduction by S_i.

$$S_i = \max|F(X_i|B) - F(X_i|\overline{B})| \quad (3)$$

Where $F(X_i|B)$ and $F(X_i|\overline{B})$ are the empirical cumulative distribution functions of the parameter (X_i) when considering the input samples associated with the behavioural and non-behavioural outputs, respectively.

A total of 59 parameters were included in the GSA study. The included parameters and their uncertainty ranges are shown in Table 1. The parameters were assumed to be uniformly distributed and the uncertainty ranges were set according as proposed by Brun et al. [32]. All parameters included in the GSA study were kinetic parameters of ASM2d-N_2O. The hydraulic WWTP parameters were not considered because they were calculated during the hydraulic characterization. The influent characterization parameters were neither included, as they were measured during the experimental data campaign. Moreover, the stoichiometric parameters of ASM2d–N_2O were assumed to be accurately known parameters and were not included in the GSA. Finally, as the Girona WWTP removes P by chemical precipitation with sodium aluminate dosage, the parameters related to Polyphosphate Accumulating Organisms (PAO) were not included.

2.6. Calibration procedure

The ASM2d-N_2O model was calibrated once the hydraulics of the Girona WWTP had been identified and the influent of the experimental data campaign had been characterized. The overall procedure followed to calibrate the model is summarized below:

1) a preliminary calibration was performed, aiming to fit the P chemical removal by sodium aluminate addition. This calibration was performed under pseudo-steady state conditions to decrease the computational cost. Thus, the experimental values collected during the experimental campaign were averaged. 2) The CCF was built with the dynamic data of nutrients and GHG emissions collected during the experimental data campaign. 3) The GSA was performed with the kinetic parameters of the ASM2d-N_2O model as input factors and the CCF as output. 4) The top five ranked parameters of the GSA were selected to build different subsets of parameters. To minimise the potential problem of model overfitting, the parameter subset size to be calibrated was set to a maximum of four parameters. 5) All the subsets were calibrated under dynamic conditions. The subset of the optimized parameters that most reduced the CCF was selected. The identifiability of each subset and the confidence interval for its parameters were evaluated based on the FIM methodology.

The aim of the preliminary calibration was to fit the sodium aluminate addition to describe the phosphate concentration in the biological reactors. During the preliminary calibration, the influent and operational dynamic data from the experimental campaign were averaged and used as model inputs (constants inputs). The phosphate concentration in the reactors were also averaged and used as output variables. The sodium aluminate addition to the IR stream was calibrated using the X_{MeOH} state variable of ASM2d-N_2O, which stands for ferric-hydroxide. Equation (4) was used as the preliminary calibration cost function (PCCF):

$$PCCF = \sqrt{\sum_{i=1}^{7} (y_{exp,i} - y_{model,i})^2} \quad (4)$$

Where: "i" is related to each sample in the biological reactor, y_{exp} is the averaged experimental phosphate concentration and y_{model} is the steady state phosphate concentration obtained after a simulation of 300 days.

Equation (5) was used to calculate the individual calibration cost function defined for each monitored variable (CCF_i) and Equation (6) was used to calculate the overall CCF:

$$CCF_i = \sum_{r=1}^{7} \sqrt{\sum_{j=1}^{n} (y_{expi,j} - y_{modeli,j})^2} \quad (5)$$

$$CCF = \sum_{i=1}^{4} CCF_i = CCF_{NH4} + CCF_{NO2} + CCF_{NO3} + CCF_{N2O} \quad (6)$$

Where: "i" is related to the output variable of interest (NH_4^+, NO_2^-, NO_3^- or N_2O); "j" is related to each experimental data point (n measures); "r" is related to each sample zone and y_{exp} and y_{model} are related to experimental data and model output, respectively. The phosphorus related variables were not added in the CCF for the reasons discussed in section 2.5.

Each dynamic simulation started with a 300-day steady-state (SS) simulation (constant inputs). Then, a 3-day dynamic simulation was performed using the SS simulation results as the initial point and the CCF was calculated using the operational data sampled during the experimental campaign. Each parameter subset was calibrated by minimising the CCF through a global searching minimization method using the Matlab function *patternsearch*. The identifiability of the subsets was evaluated using the FIM methodology [33,34], which was applied to calculate the confidence interval for each parameter, D criteria (CritD), modified E criteria (CritModE), normalized D criteria (NormD) and the ratio between NormD and CritModE (RDE), as detailed in Section S6 of the SI.

The goodness of the model fit for N_2O emissions was quantitatively assessed with the performance metrics detailed in equations (7) to (10) [35], where y_i, $\bar{y}$, $\hat{y}_i$ and n refer to the experimental values, their average, the model prediction and the number of measurements, respectively.

$$R^2 = \frac{\sum_{i=1}^{n}(\hat{y}_i - \bar{y})^2}{\sum_{i=1}^{n}(y_i - \bar{y})^2} \quad (7)$$

$$RMSE = \sqrt{\frac{\sum_{i=1}^{n}(y_i - \hat{y}_i)^2}{n}} \quad (8)$$

$$MAE = \frac{1}{n}\sum_{i=1}^{n}|y_i - \hat{y}_i| \quad (9)$$

$$Bias = \frac{1}{n}\sum_{i=1}^{n}(y_i - \hat{y}_i) \quad (10)$$

The experimental campaign lasted three days. In addition, the gas collection system could only analyse one aerobic zone at a time and, unfortunately, the system failed during one night due to the gas measurement computer was powered off. Therefore, in the absence of a large

dynamic data set, all available data from this experimental campaign were used for the calibration process. The validation was performed with data selected from a previous N_2O measuring campaign in the same WWTP [21]. Specifically, the data used for model validation were the N_2O emissions and the ammonium profiles measured in the AER2 compartment of the WWTP during 15–21 November 2016 and reported in a previous experimental work [21]. The validation procedure and results are detailed in section S8 of the SI.

3. Results and discussion

3.1. Experimental data and plant performance

The NH_4^+, NO_2^-, NO_3^- and PO_4^{3-} profiles in the influent and in each compartment are shown in Figures S2 to S5 in section S2 of the SI. The influent temperature and pH were approximately constant during the experimental campaign at 24.4 ± 0.5 °C and 7.44 ± 0.09, respectively. Good plant performance was achieved, obtaining a COD removal of 96% and higher than 99% for total Kjeldahl nitrogen (TKN) and P. Mean DO values were 1.8, 1.5, 1.2 and 2.0 g O_2 m^{-3} in AER1 to AER4 compartments, respectively. Nitrite concentrations were below 0.25 g N m^{-3} in all compartments, with averaged ammonium and nitrate concentrations in the last compartment of 0.1 g N m^{-3} and 3.3 g N m^{-3}, respectively, showing high AOB and NOB activity. Figure S5 shows that the PO_4^{3-} concentration only increased on average by 2.5 g P m^{-3} in the anaerobic reactor (ANA1), compared to the PO_4^{3-} concentration in the influent, showing a low PAO activity. Hence, the addition of chemical P precipitant probably limited the PAO activity.

The COD fractionation characterization (i.e. the calculation of the COD model state variables from the measured variables) was performed on the basis of the effluent filtered COD ($COD_{fil,eff}$) and three different influent COD measurements: total COD (COD_{tot}), filtered COD at 1.2 μm (COD_{fil}) and flocculated-filtered COD at 0.45 μm (COD_{sol}). More details on this procedure, the list of all determined model influent state variables and the COD influent profiles can be found in section S3 of the SI. The influent fractionation was assumed constant during the dynamic calibration.

Fig. 2 shows the N_2O emissions from the first three aerated zones (AER1 to AER3) together with the ammonium concentration profile obtained from analytical tests and from an online sensor in AER2. The grey area in Fig. 2 indicates that N_2O data was not available due to a technical failure. Similar peak profiles of N_2O emissions were observed for the other three aerobic reactors monitored. However, the amount of N_2O emitted was different, with AER1 being the compartment with highest emissions and AER3 with the lowest. This could be related to the fact that higher ammonium concentrations were present in AER1, that led to higher ammonium oxidation rates. Furthermore, Fig. 2 shows that N_2O emissions were related to ammonium concentration and thus emissions decreased to negligible levels when ammonium was depleted. The same pattern of N_2O peak emissions were reported in other studies in full-scale WWTPs or in lab experiments with nitrifying-enriched sludge [26,36]. The peak is attributed to the sudden increase of ammonium, which produces a transient between low-activity to high-activity of nitrifying biomass [4,9,26]. During the experimental campaign, the averaged N_2O emission factor (N_2O-EF) (calculated as the percentage of the influent TKN load emitted as N_2O-N), of AER1 to AER3 reactors was 0.41%, which is in the low range of the N_2O-EF reported for full-scale WWTPs [4,9,12,26]. However, the calculated N_2O-EF was slightly higher than the N_2O-EF calculated during a large monitoring campaign at the same WWTP, N_2O-EF of 0–0.13% [26]. The increase in N_2O-EF can be due to the multiple factors that can be found in an urban WWTP, such as operational parameters (e.g. temperature, DO, pH and recycling flows) and changes in wastewater flow and composition (e.g. nitrogen concentration, COD concentration and fractionation, and increase in the fraction of industrial wastewater) [12].

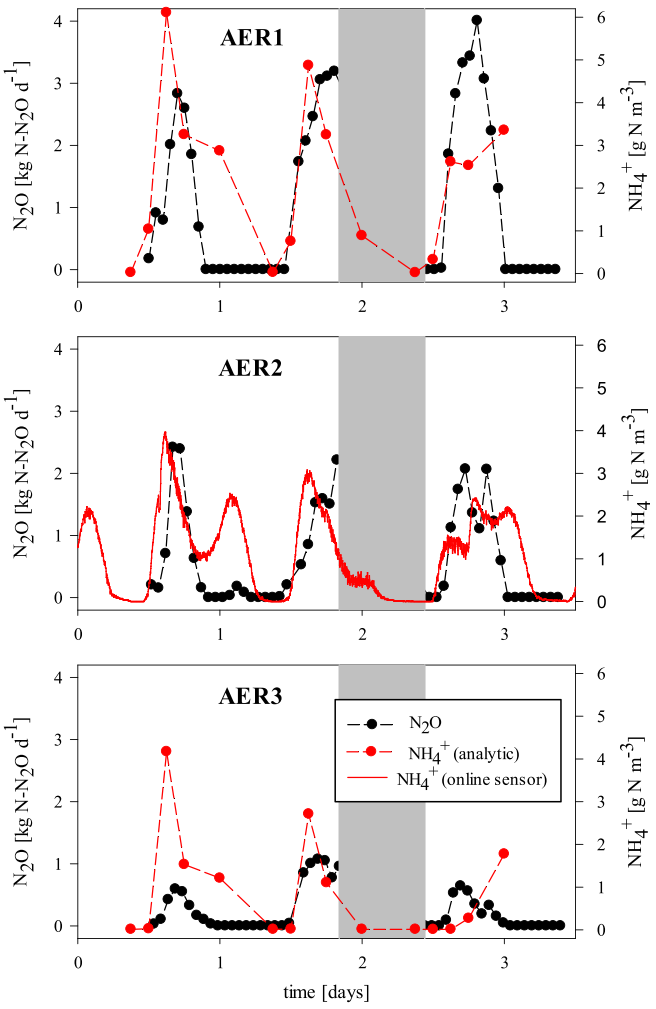

Fig. 2. Measured N_2O emissions and NH_4^+ concentration in compartments AER1, AER2 and AER3. The grey area represents a technical failure in the N_2O gas measurement system. The dashed line at the N_2O and NH_4^+ analytical data points is an aid for better visualization of the experimental profiles.

3.2. Hydraulic characterization

The pulse response at the influent of biological reactors and the flowrates measured during the RTD experiment are shown in Fig. 3. The influent tracer concentration, the flowrates and the dimensional data of the Girona WWTP were used as model inputs to characterize the hydraulics of the plant.

Fig. 4 shows the experimental bromide concentrations measured during the tracer test. The concentration of Br^- before the KBr pulse was not negligible. Therefore, a constant inlet bromide concentration of 0.0627 g m^{-3} was considered during the experiment. A tracer mass balance over the secondary treatment after 78 h showed that a 79% of the total tracer introduced was detected at the output and that 3.5 kg of the injected Br^- remained in the reactor when the experiment was stopped.

The initial assumption that each reactor operated as an ideal CSTR was correct, as the trends of the model predictions agreed with the experimental values. However, the assumption that the secondary settler flow pattern was also a CSTR was false and therefore the model was revised. The parameters to be estimated were the number of N tanks-in-series of the secondary settler and the percentage distribution of the influent flow between each biological line (i.e. f_{Q1} and f_{Q2}, where f_{Q1} and f_{Q2} are the percentage of the influent flow going to the first and second biological treatment lines, respectively, and $f_{Q1} + f_{Q2} = 1$).

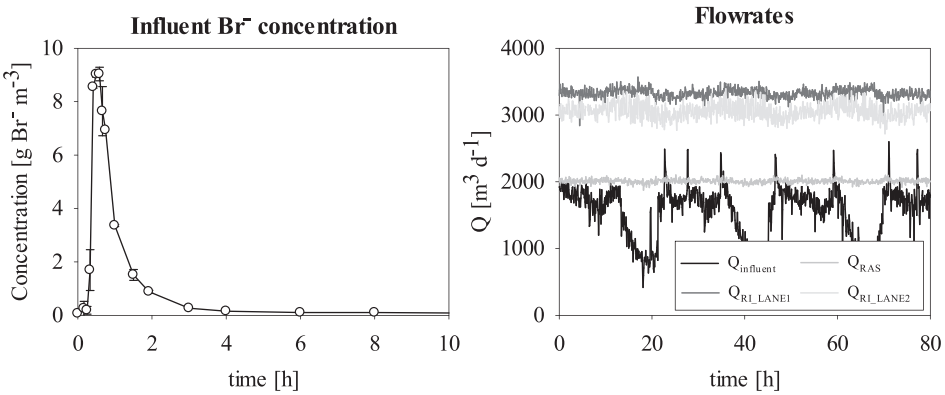

Fig. 3. Pulse response concentration measured in the effluent of the primary clarifier (influent of the biological reactors) and flowrates measured during the tracer experiment.

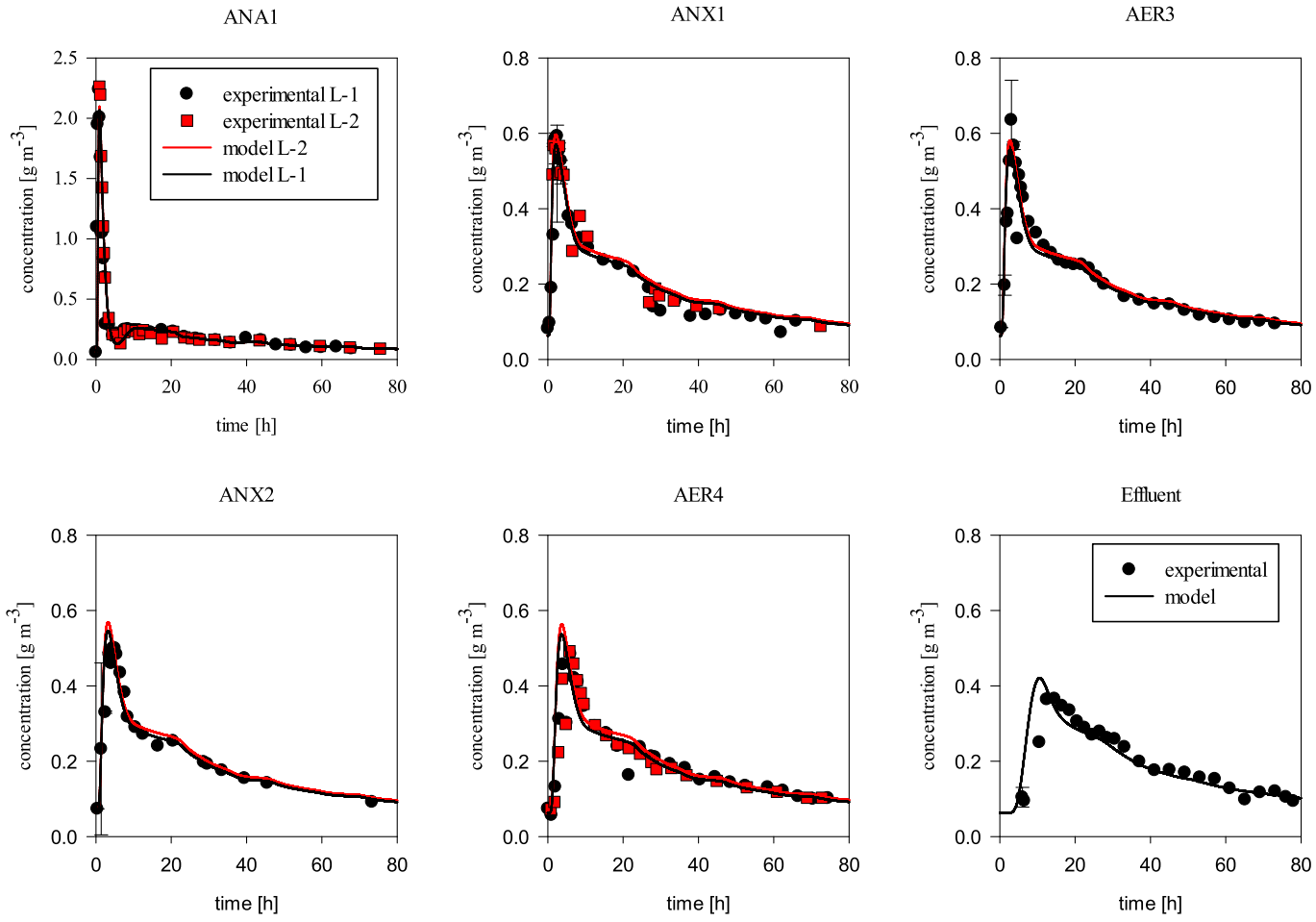

Fig. 4. Tracer experiment results and model results in each measured compartment and in the effluent.

Fig. 4 shows the results obtained during the hydraulic calibration. The model accurately described the trends of the experimental data. The optimized parameters for the secondary settler flow pattern were N = 5 tanks and hence the secondary settler flow pattern was closer to a plug flow reactor flux model than to a CSTR. The flowrate was distributed approximately equally between the two lines, with 49.33% of the influent flowrate going to the first biological treatment line and 50.67% to the second treatment line. These results contradicted the initial thinking of the plant operators that the distribution was not symmetrical.

3.3. Preliminary calibration

The next step after the identification of the WWTP hydraulics was the calibration of the kinetic model ASM2d-N_2O. As the flow distribution between both biological treatment lines was approximately the same, only one biological treatment line was considered in the kinetic calibration and in the GSA studies. The preliminary calibration (see section 2.6) aimed to reduce structural discrepancies between the model and the experimental variables [37], particularly for those related to P, before performing the GSA and the subsequent dynamic calibration.

The X_{MeOH} addition that minimized the PCCF was 184 kg $Fe(OH)_3$ d^{-1}. The PCCF obtained was 2.7, achieving a reduction of 74% compared to the PCCF before the preliminary calibration. The fits obtained on the average phosphate concentration are shown in Figure S7 of section S4 of the SI. With this addition of X_{MeOH}, the model was found to predict that the percentage of P biologically removed by PAO was 24%. The calibrated X_{MeOH} addition value was maintained constant during all dynamic simulations. Moreover, as phosphate concentrations were calibrated by chemical precipitation, PAO-related parameters were not considered during the ASM2d–N_2O calibration and phosphate concentrations were not considered in the CCF, i.e. the PAO-related parameters were maintained at their default values in all dynamic simulations.

3.4. Development of the calibration cost function (CCF)

The data obtained during the experimental campaign were used to dynamically calibrate the ASM2d-N_2O model to the Girona WWTP. In total, four variables were included in the cost function and considered as the output variables of interest: ammonium, nitrite and nitrate in the biological reactors and N_2O emissions from AER1 to AER3. Therefore, the CCF was divided into four different cost functions (CCF_i) for each output variable of interest (i.e. CCF_{NH4}, CCF_{NO2}, CCF_{NO3}, CCF_{N2O}). The overall CCF (Equation (6)) was calculated as the sum of each individual output variable CCF_i (Equation (5)). As all the CCF_i were of the same order of magnitude, no weighting factors were included in the CCF calculation.

3.5. Global sensitivity analysis

A number of N = 2000 simulations was selected for the MC experiment. The CCF and each CCF_i for each simulation were then evaluated and discretized into two populations, B and $\overline{B}$ (see section 2.5). The threshold fixed to discretize the CCF (and the associated input parameters) was the maximum reduction on the CCF that can be achieved with a number of simulations of the behavioural group of at least $N_B = 100$, representing 5% of all simulations. The maximum reduction in CCF that satisfied the requirement of $N_B = 100$, and therefore, the threshold selected for GSA evaluation was 40%, compared to the CCF calculated with the default parameter values of ASM2d-N_2O. For this selected threshold, the top ranked GSA indices are shown in Table 2. Table S2 in section S5 of the SI shows the full rank of parameters evaluated.

Among the CCF_i-related results, a high reduction threshold of around 80% was found for nitrite and nitrous oxide CCFs. On the other hand, the thresholds found for the ammonium and nitrate CCFs were around 10%. These results showed that the maximum reduction in the overall CCF that could be achieved was related to the reduction in the nitrite and nitrous oxide CCFs. The initial simulations agreed with this observation, as the predicted ammonium and nitrate concentrations trends agreed with the experimental values. In addition, Table 2 shows that the five top ranked parameters were related to nitrification processes, more specifically to the nitratation process, as four of the five top ranked parameters were related to NOB (μ_{NOB}, b_{NOB}, K_{NO2_NOB} and K_{O2_NOB}) and the other parameter was related to AOB bacteria (q_{AOB_AMO}). Therefore, the GSA results showed that the ASM2d-N_2O model calibration for the Girona WWTP should focus on the calibration of the nitrifying bacteria parameters, which is not surprising. However, in view of good modelling practices, a systematic methodology to understand the parameter sensitivity should always be incorporated, particularly when there are a high number of parameters. In this case, i.e. for this model, specific WWTP operational conditions and available experimental data, these results allowed to detect the most sensitive parameter among all those related to the biological nitrogen removal process and confirmed that any unexpected parameter had a high sensitivity on N_2O measurements.

Table 2
Ranking of the first twenty parameters obtained in the GSA.

Position	Parameter	Description
1	μ_{NOB}	Maximum NOB growth rate
2	b_{NOB}	Decay rate of NOB
3	K_{NO2_NOB}	Saturation coefficient for NO_2^-
4	q_{AOB_AMO}	Maximum rate for the AMO reaction
5	K_{O2_NOB}	Half-saturation coefficient for O_2
6	n_{G5}	Anoxic growth factor ($N_2O \rightarrow N_2$)
7	K_{OH5}	Half-saturation coefficient for O_2
8	q_{AOB_HAO}	Maximum rate for HAO reaction
9	$q_{AOB\_N2O\_ND}$	Maximum N_2O production rate by the ND pathway
10	K_{NO2}	Saturation/inhibition coefficient for NO_2^-
11	K_{I5NO}	NO inhibition coefficient ($N_2O \rightarrow N_2$)
12	$K_{I\_O2\_AOB}$	N_2O constant for production inhibition by O_2
13	K_{O2_AOB1}	AOB affinity constant for O_2 (AMO reaction)
14	n_{G3}	Anoxic growth factor ($NO_2^- \rightarrow NO$)
15	K_{S5}	Half-saturation coefficient for substrate
16	K_{NO2_Den}	Half-saturation coefficient for NO_2^-
17	K_{I4NO}	NO inhibition coefficient ($NO \rightarrow N_2O$)
18	K_{ALK}	Saturation coefficient for alkalinity (HCO_3^-)
19	K_{HNO2_AOB}	AOB affinity constant for HNO_2
20	K_{NO3_H}	Saturation/inhibition coefficient for NO_3^-

3.6. Dynamic calibration

The dynamic calibration was conducted after identifying the ASM2d-N_2O parameters most likely to reduce the CCF. Different parameter subsets were defined with all the possible combinations of the five top ranked parameters from the GSA (Table 2). The size of parameter subsets ranged from one to four parameters, resulting in a total of 30 parameter subsets to be calibrated (Table S3 in SI). The parameter subset and calibrated values that most reduced the CCF were $\mu_{NOB} = 0.674 \pm 0.019$ d^{-1}, $q_{AOB\_AMO} = 5.517 \pm 0.058$ gN $(gCOD)^{-1}$ d^{-1}, $K_{O2\_NOB} = 0.126 \pm 0.029$ gO_2 m^{-3} and $K_{NO2\_NOB} = 0.126 \pm 0.030$ gN m^{-3}. The CCF was reduced by 53.3% with this parameter subset, compared to the CCF after preliminary calibration, mainly due to the reduction of the CCF of NO_2^- and N_2O (87.7 and 86.5%, respectively). The fit between experimental data and model predictions for N-species is shown in Fig. 5 and those for N_2O emissions are shown in Fig. 6.

The calibration results for each subset of parameters can be found in Table S3 of the SI. The selected subset shows low confidence interval values for all parameters and a parameter confidence interval norm of 33.6%, which is the lowest of all subsets with four parameters. It also provides a high NormD = 9.8 10^{17}, a low CritModE = 809 and the highest RDE = $1.22 \cdot 10^{15}$. These values, compared to those of the other subsets, indicate that the selected subset has a good identifiability linked to the ability to provide a low CCF. In contrast, the subset μ_{NOB}, b_{NOB}, q_{AOB_AMO}, K_{O2_NOB} also provides a very similar CCF, but it has an extremely high parameter confidence interval for b_{NOB} (1211%), i.e. $b_{NOB} = 0.0008 \pm 0.0095$ d^{-1}, which shows the low identifiability of this parameter. The problem of a much higher confidence interval than the parameter value with b_{NOB} also appears in all subsets where very low b_{NOB} values are obtained during the optimization. This indicates that, with the experimental information available in this study, it would not be advisable to use b_{NOB} for model fitting. In fact, this is the only parameter of the initial five that is not included in the chosen subset.

Regarding the predictions obtained, the model reasonably predicts the concentration trends of the different N-species in the reactor. The ASM2d-N_2O was able to explain the low nitrite concentrations measured during the experimental campaign, by reducing the NOB oxygen and nitrite affinity constants with respect to the default values [16]. Experimental nitrate data and model fits showed a discrepancy in nitrification capacity, as measured nitrate showed smaller increases among aerobic reactors (AER1 to AER3) compared to model predictions. The model could not predict such a high degree of simultaneous nitrification and denitrification occurring in AER2 and AER3. This was due to the low DO levels in AER2 and AER3 (1.5 and 1.2 g O_2 m^{-3}, respectively) in addition

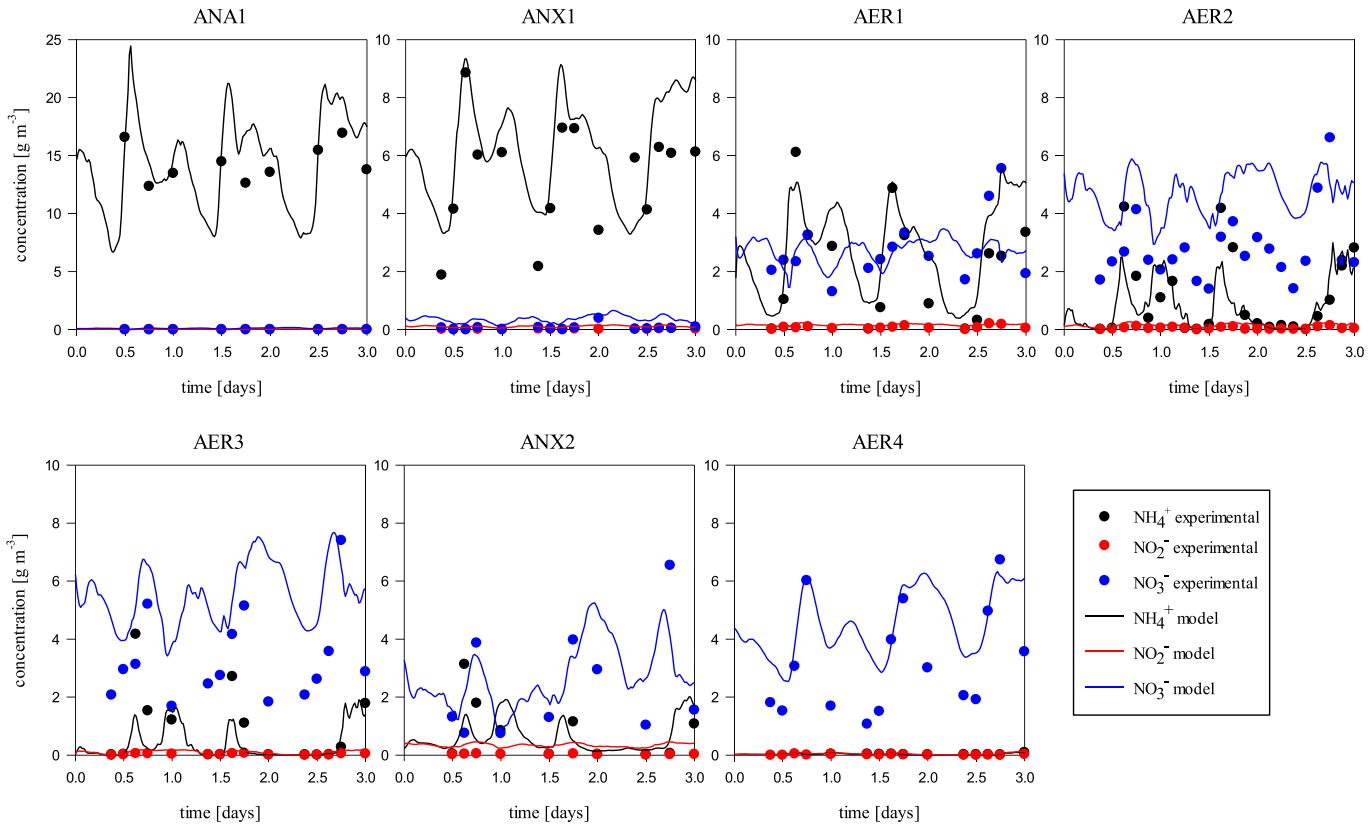

Fig. 5. Concentrations of ammonium, nitrite and nitrate measured during the experimental campaign and fit obtained during the dynamic calibration of ASM2d-N_2O.

to the inherent instability of the DO control system in the plant, which caused significant noise in the DO concentration and favoured denitrification processes when the DO concentration was low.

On the other hand, the goodness of the ASM2d-N_2O fit for N_2O experimental data was evaluated in more detail. Statistical model fit criteria were calculated for each reactor (Table 3) as detailed in section 2.6. The coefficient of determination was low in the three reactors (R^2 = 0.107, 0.518 and 0.533), indicating that the model could only partially describe the experimental results. The highest RMSE value resulted in AER1, but when comparing the RMSE with the average experimental value ($\bar{y}$), the error was 85%, 79% and 139% for reactors AER1, AER2 and AER3 respectively. The MAE results were similar to those of RMSE, obtaining the highest value for AER1. Finally, the model bias was negative for all three reactors (Bias = 0.114, -0.285 and -0.120), indicating a slight model underestimation of N_2O emissions. Despite the statistical values discussed above, the model was able to reasonably capture the dynamics and range of N_2O emissions in AER2 and AER3 (Fig. 6), except for the period 1.0–1.5 d, where unexpectedly low N_2O values were registered by the online measuring system in all three reactors. These reasonable predictions were obtained even considering that only one parameter related to biomass producing N_2O was modified (q_{AOB_AMO}) and also taking into account the intrinsic operational variability observed in full-scale WWTPs.

Going into more detail with respect to the discrepancy of N_2O emissions in the period 1.0–1.5d, the model predicted a peak of ammonium during this period that was not experimentally detected (Fig. 5). The model predictions of N_2O emissions during this second daily peak of ammonium were mostly related to the ND pathway, since, as a result of the ammonium accumulation, the model also predicted a slight accumulation of hydroxylamine up to 0.9 g N m^{-3} (three times the affinity constant of AOB), which is the electron acceptor substrate for the ND pathway. Moreover, the model predicted the highest nitrite concentration in AER1, obtaining an average value of 0.17 g N m^{-3} during the three days of dynamic simulation. This a priori low nitrite concentration was high enough to support the ND pathway in this reactor, thus causing the overestimation of N_2O emissions.

ND is the biological N_2O production pathway responsible for most of emissions during wastewater treatment [9,12,16,38]. In fact, the average contribution of the ND pathway to the total N_2O production in AER1 was 82% and decreased to 78% and 48% in AER2 and AER3, respectively (see Figure S8 in SI). These values are in agreement with literature ranges for aerobic reactors [38]. The NN pathway contributed 6% to the total N_2O production and the HD pathway contributed mostly in AER3 with 45% (Figure S8 in SI), where the DO was the lowest of the aerobic zones (1.2 g O_2 m^{-3}). The higher contribution of the HD pathway in AER3 shows that simultaneous nitrification and denitrification occurred in this reactor due to the low DO coupled with low NH_4^+ and high NO_3^- concentrations. The predicted N_2O-EF, only considering AER1 to AER3 zones, was 0.55% which is very similar to the measured one (0.41%).

Although the model predictions are in line with previous work in the literature, it should be noted that biological N_2O production are complex processes with several metabolic pathways with challenging interactions that have probably not been fully revealed. There is a lack of a consensus model describing all the scenarios and, thus, the biological model used may not be capable to describe all the particular cases. The ASM2d-N_2O model contains several assumptions and short-cuts in order to describe full-scale N_2O emissions in a simple way. For instance, the ASM2d-N_2O model assumes that the AOB-driven nitrite reduction to N_2O is a one-step process to avoid a NO loop [16] based on the original structure [14] that was only focused on AOB metabolism. Likewise, the quantity and quality dataset used for calibration corresponds to a relatively short-term period and, as such, we missed rain-events or periods with changing temperature or variable flow. Therefore, these

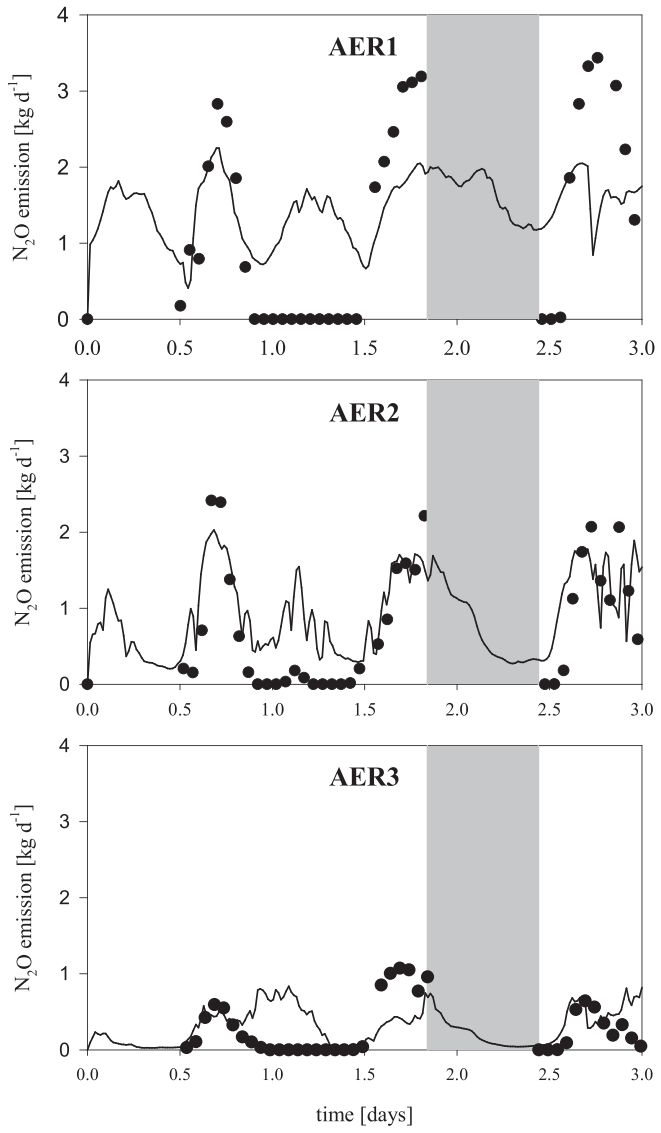

Fig. 6. N_2O emissions measured during the experimental campaign and fits obtained during the dynamic calibration of ASM2d-N_2O. In the grey area no experimental N_2O emission data were available due to a technical failure.

Table 3
Performance criteria to assess the goodness of fit for N_2O predictions.

	n	R^2	$\bar{y}$	RMSE	MAE	Bias
AER1 reactor	37	0.107	1.339	1.141	1.014	−0.114
AER2 reactor	37	0.518	0.763	0.603	0.514	−0.285
AER3 reactor	38	0.533	0.289	0.401	0.310	−0.120

considerations, i.e. the model structure and the quantity/quality of the calibration dataset, may have a strong influence on the parameter subset selection, parameter estimates and model predictions, and should be taken into account when analysing the results obtained, considering also the possible model limitations when it is to be applied to other scenarios.

4. Model exploitation

Once the dynamic calibration and the model validation (Section S8 in SI) were done, two scenarios were simulated to investigate the effect on N_2O emissions and N_2O-EF of varying the flowrate distribution between both treatment lines (Fig. 1). In the first case, an equal flow distribution was simulated, i.e. 50% of the influent flowrate was fed to each line, according to the tracer experiments results (section 3.2). The second case was modelled assuming that 40% of the influent flowrate went to the first treatment line and the remaining 60% to the second one. This study was performed to assess the possible effect than an incorrect flow distribution between treatment lines had on the N_2O emissions due to possible treatment line overloading and changes in treatment plant loads. Each simulation was done following the same methodology as in the dynamic calibration (section 2.6) and with the same model inputs. In addition, it was assumed that the aeration system was able to maintain the same DO concentration despite the increase of N load.

Fig. 7 shows the predicted N_2O emissions in each treatment line and the total N_2O emissions and N_2O-EF for each case. Fig. 7A shows that the predicted N_2O emissions from the treatment lines increased with increasing influent flowrate. The average N_2O emission rate obtained for an influent flowrate distribution of 40, 50 and 60% were 2.5, 3.2 and 3.8 kg N_2O-N d^{-1} respectively. The same ammonium was obtained in the effluent for all three influent distribution simulations, however, nitrite and nitrate in the effluent increased with increasing influent flowrate due to the increase on the TKN influent load. Fig. 7A reveals that the same total N_2O emissions were predicted for both cases (6.3 kg N_2O-N d^{-1}). This is because the N_2O emissions increased linearly with increasing influent flowrate and therefore the total N_2O emissions for both cases were the same. Fig. 7B also shows that the predicted N_2O-EF for both lines was the same for each case because the N_2O emissions increased with the same slope as the TKN removed. Therefore, these simulations show that if one of the two lines was overloaded, emissions would increase in that line, but these higher emissions would be compensated to the same extent by the lower emissions in the underloaded line. Thus, the plant, would not suffer an increase in total N_2O emissions even if the flow distribution was not entirely correct, as long

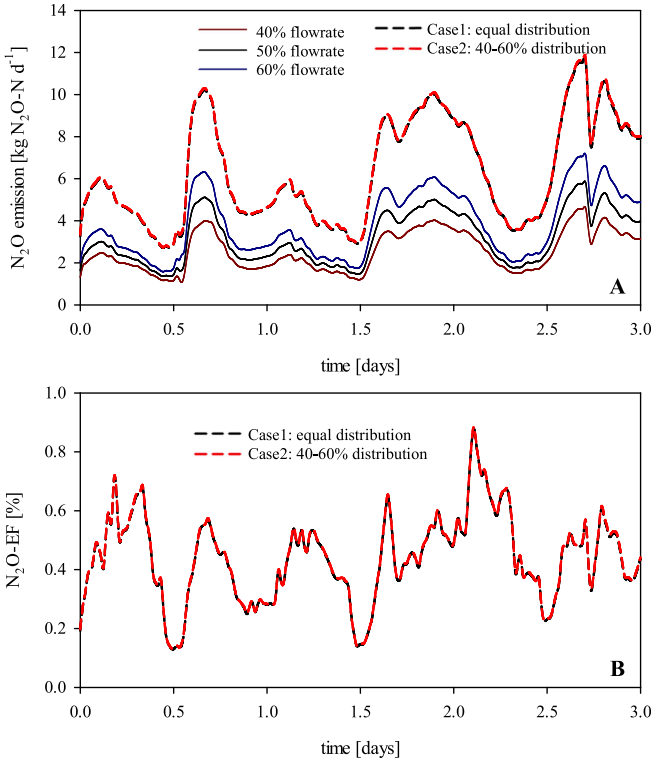

Fig. 7. Predicted N_2O emissions in two different flowrate scenarios: Case 1 (equal influent flowrate distribution in both treatment lines) and Case 2 (40–60% influent flowrate distribution). (A) N_2O emissions in each treatment line for 40%-50%-60% flowrate and total N_2O emissions. (B) Predicted N_2O-EF for both cases.

as it can be ensured that the aeration system is capable of providing sufficient oxygen to maintain the DO around the setpoint. For scenarios where there is no oxygen control and constant aeration is used, an increase in ammonium loading may decrease the DO concentration, moving the operating point to one with higher N_2O production, which would increase emissions as previously studied [16].

5. Conclusions

This work is a comprehensive calibration of the ASM2d-N_2O model to a full-scale WWTP including hydraulics with the following main findings:

- Modelling the flow patterns in the plant is very interesting in view of its calibration. The tracer experiment showed that all reactors of the two treatment lines had a correct hydraulic behaviour, as no dead volumes, flux recycling or by-passes were found. Furthermore, it was demonstrated that an equal flow was flowing to each line.
- A GSA method (RSA) was successfully applied to rank the parameters most likely to reduce the CCF. The sensitivity analysis revealed that the top ranked parameters were related to nitrifying organisms.
- The dynamic kinetic calibration of ASM2d-N_2O correctly captures the trends of N-species in the reactors, only by modifying four kinetic parameters.
- The N_2O-EF predicted was very similar to that measured experimentally and the emission profiles trends were in general in agreement with the experimental data.
- The simulations revealed that, under current plant operating conditions, an increase in flow in one of the treatment lines would increase N_2O emissions in that overloaded line, but would be offset by a decrease in the underloaded line, so that total emissions would not vary significantly, provided the control system was able to maintain the operating DO.

Declaration of Competing Interest

The authors declare that they have no known competing financial interests or personal relationships that could have appeared to influence the work reported in this paper.

Acknowledgements

Borja Solís is grateful for the PIF PhD grant funded by Universitat Autònoma de Barcelona. Borja Solís, Albert Guisasola and Juan Antonio Baeza are members of the GENOCOV research group (Grup de Recerca Consolidat de la Generalitat de Catalunya, 2017 SGR 1175, www.genocov.com) and were supported by the European Union's Horizon 2020 research and innovation program under the Marie Skłodowska-Curie C-FOOT-CTRL project (grant agreement No 645769). M. Pijuan and Ll. Corominas acknowledge the support from the Economy and Knowledge Department of the Catalan Government through a Consolidated Research Group (ICRA-TECH - 2017 SGR 1318) - Catalan Institute for Water Research. A special thanks to Ms. Cristina Pujol and Mr. Lluís Ayach from TRARGISA, the company responsible for the operation of the WWTP for all the help during the monitoring campaign. We acknowledge the contribution of Dr. Ayla Kiser (www.aylakiser.com) in the design and execution of the tracer test.

Appendix A. Supplementary data

Supplementary data to this article can be found online at https://doi.org/10.1016/j.cej.2022.134733.

References

[1] IPCC, 2014: Climate Change 2014: Synthesis Report . Contribution of Working Groups I, II and III to the Fifth Assessment Report of the Intergovernmental Panel on Climate Change [Core Writing Team, R.K. Pachauri and L.A. Meyer (eds.)]. IPCC, Geneva, Switze, (n.d.).
[2] D.J.I. Gustavsson, S. Tumlin, Carbon footprints of Scandinavian wastewater treatment plants, Water Sci. Technol. 68 (2013) 887–893, https://doi.org/10.2166/wst.2013.318.
[3] A.R. Ravishankara, J.S. Daniel, R.W. Portmann, Nitrous Oxide (N 2 O): The Dominant Ozone-Depleting Substance Emitted in the 21st Century, Science 326 (5949) (2009) 123–125, https://doi.org/10.1126/science.1176985.
[4] M.J. Kampschreur, H. Temmink, R. Kleerebezem, M.S.M. Jetten, M.C.M. van Loosdrecht, Nitrous oxide emission during wastewater treatment, Water Res. 43 (17) (2009) 4093–4103, https://doi.org/10.1016/j.watres.2009.03.001.
[5] J. Foley, D. de Haas, Z. Yuan, P. Lant, Nitrous oxide generation in full-scale biological nutrient removal wastewater treatment plants, Water Res. 44 (3) (2010) 831–844, https://doi.org/10.1016/j.watres.2009.10.033.
[6] B.-J. Ni, Z. Yuan, Recent advances in mathematical modeling of nitrous oxides emissions from wastewater treatment processes, Water Res. 87 (2015) 336–346, https://doi.org/10.1016/j.watres.2015.09.049.
[7] J.D. Caranto, K.M. Lancaster, Nitric oxide is an obligate bacterial nitrification intermediate produced by hydroxylamine oxidoreductase, Proc. Natl. Acad. Sci. 114 (31) (2017) 8217–8222, https://doi.org/10.1073/pnas.1704504114.
[8] P. Wunderlin, J. Mohn, A. Joss, L. Emmenegger, H. Siegrist, Mechanisms of N2O production in biological wastewater treatment under nitrifying and denitrifying conditions, Water Res. 46 (4) (2012) 1027–1037, https://doi.org/10.1016/j.watres.2011.11.080.
[9] Y. Law, L. Ye, Y. Pan, Z. Yuan, Nitrous oxide emissions from wastewater treatment processes, Philos. Trans. R. Soc. B Biol. Sci. 367 (1593) (2012) 1265–1277, https://doi.org/10.1098/rstb.2011.0317.
[10] M. Henze, W. Gujer, T. Mino, M.C.M. van Loosdrecht, Activated Sludge Models ASM1, ASM2, ASM2d and ASM3, Scientific and technical report No 9, IWA Publishing (2000), https://doi.org/10.2166/9781780402369.
[11] B.-J. Ni, L. Ye, Y. Law, C. Byers, Z. Yuan, Mathematical modeling of nitrous oxide (N2O) emissions from full-scale wastewater treatment plants, Environ. Sci. Technol. 47 (14) (2013) 7795–7803, https://doi.org/10.1021/es4005398.
[12] T.M. Massara, S. Malamis, A. Guisasola, J.A. Baeza, C. Noutsopoulos, E. Katsou, A review on nitrous oxide (N2O) emissions during biological nutrient removal from municipal wastewater and sludge reject water, Sci. Total Environ. 596-597 (2017) 106–123, https://doi.org/10.1016/j.scitotenv.2017.03.191.
[13] B.-J. Ni, Z. Yuan, K. Chandran, P.A. Vanrolleghem, S. Murthy, Evaluating four mathematical models for nitrous oxide production by autotrophic ammonia-oxidizing bacteria, Biotechnol. Bioeng. 110 (1) (2013) 153–163, https://doi.org/10.1002/bit.24620.
[14] M. Pocquet, Z. Wu, I. Queinnec, M. Spérandio, A two pathway model for N_2O emissions by ammonium oxidizing bacteria supported by the NO/N_2O variation, Water Res. 88 (2016) 948–959, https://doi.org/10.1016/j.watres.2015.11.029.
[15] C. Domingo-Félez, B.F. Smets, A consilience model to describe N_2O production during biological N removal, Environ. Sci. Water Res. Technol. 2 (6) (2016) 923–930, https://doi.org/10.1039/C6EW00179C.
[16] T.M. Massara, B. Solís, A. Guisasola, E. Katsou, J.A. Baeza, Development of an ASM2d-N2O model to describe nitrous oxide emissions in municipal WWTPs under dynamic conditions, Chem. Eng. J. 335 (2018) 185–196, https://doi.org/10.1016/j.cej.2017.10.119.
[17] M. Gresch, D. Braun, W. Gujer, The role of the flow pattern in wastewater aeration tanks, Water Sci. Technol. 61 (2010) 407–414, https://doi.org/10.2166/wst.2010.803.
[18] D. Olivet, J. Valls, M.À. Gordillo, À. Freixó, A. Sánchez, Application of residence time distribution technique to the study of the hydrodynamic behaviour of a full-scale wastewater treatment plant plug-flow bioreactor, J. Chem. Technol. Biotechnol. 80 (4) (2005) 425–432, https://doi.org/10.1002/jctb.1201.
[19] F. Wang, J. Li, D. Bian, Z. Nie, S. Ai, X.i. Tian, H. Wang, Effect of hydraulic residence time and inlet flow distribution ratio on the pollutant removal of low-temperature municipal wastewater in multistage AO process, Water Environ. J. 34 (S1) (2020) 742–752, https://doi.org/10.1111/wej.12574.
[20] F. Sánchez, A. Viedma, A.S. Kaiser, Hydraulic characterization of an activated sludge reactor with recycling system by tracer experiment and analytical models, Water Res. 101 (2016) 382–392, https://doi.org/10.1016/j.watres.2016.05.094.
[21] M.C. Collivignarelli, M. Carnevale Miino, S. Manenti, S. Todeschini, E. Sperone, G. Cavallo, A. Abbà, Identification and localization of hydrodynamic anomalies in a real wastewater treatment plant by an integrated approach: RTD-CFD Analysis, Environ. Process. 7 (2) (2020) 563–578, https://doi.org/10.1007/s40710-020-00437-4.
[22] M. Majewsky, T. Gallé, M. Bayerle, R. Goel, K. Fischer, P.A. Vanrolleghem, Xenobiotic removal efficiencies in wastewater treatment plants: Residence time distributions as a guiding principle for sampling strategies, Water Res. 45 (18) (2011) 6152–6162, https://doi.org/10.1016/j.watres.2011.09.005.
[23] G. Tchobanoglous, F. Burton, H.D. Stensel, Wastewater engineering: Treatment and reuse, Am. Water Work. Assoc. J. 95 (2003) 201.
[24] F. Coen, B. Petersen, P.A. Vanrolleghem, B. Vanderhaegen, M. Henze, Model-based characterisation of hydraulic, kinetic and influent properties of an industrial WWTP, Water Sci. Technol. 37 (1998) 317–326, https://doi.org/10.1016/S0273-1223(98)00352-7.
[25] P.A. Vanrolleghem, G. Insel, B. Petersen, G. Sin, D. De Pauw, I. Nopens, H. Dovermann, S. Weijers, K. Gernaey, A comprehensive model calibration

procedure for activated sludge models, Proc. Water. Environ. Fed. 2003 (9) (2003) 210–237, https://doi.org/10.2175/193864703784639615.
[26] A. Ribera-Guardia, L. Bosch, L. Corominas, M. Pijuan, Nitrous oxide and methane emissions from a plug-flow full-scale bioreactor and assessment of its carbon footprint, J. Clean. Prod. 212 (2019) 162–172, https://doi.org/10.1016/j.jclepro.2018.11.286.
[27] W.C. Hiatt, C.P.L. Grady, An updated process model for carbon oxidation, nitrification, and denitrification, Water Environ. Res. 80 (11) (2008) 2145–2156, https://doi.org/10.2175/106143008X304776.
[28] A. Saltelli, M. Ratto, S. Tarantola, F. Campolongo, Sensitivity analysis for chemical models, Chem. Rev. 105 (7) (2005) 2811–2828, https://doi.org/10.1021/cr040659d.
[29] A. Saltelli, M. Ratto, S. Tarantola, F. Campolongo, Sensitivity analysis practice: A guide to scientific models (2004), https://doi.org/10.1016/j.ress.2005.11.014.
[30] A. Saltelli, M. Ratto, T. Andres, F. Campolongo, J. Cariboni, D. Gatelli, M. Saisana, S. Tarantola, Global Sensitivity Analysis: The Primer (2008), https://doi.org/10.1111/j.1751-5823.2008.00062_17.x.
[31] F. Pianosi, K. Beven, J. Freer, J.W. Hall, J. Rougier, D.B. Stephenson, T. Wagener, Sensitivity analysis of environmental models: A systematic review with practical workflow, Environ. Model. Softw. 79 (2016) 214–232, https://doi.org/10.1016/j.envsoft.2016.02.008.
[32] R. Brun, M. Kühni, H. Siegrist, W. Gujer, P. Reichert, Practical identifiability of ASM2d parameters - Systematic selection and tuning of parameter subsets, Water Res. 36 (16) (2002) 4113–4127, https://doi.org/10.1016/S0043-1354(02)00104-5.
[33] V.C. Machado, G. Tapia, D. Gabriel, J. Lafuente, J.A. Baeza, Systematic identifiability study based on the Fisher Information Matrix for reducing the number of parameters calibration of an activated sludge model, Environ. Model. Softw. 24 (11) (2009) 1274–1284, https://doi.org/10.1016/j.envsoft.2009.05.001.
[34] A. Guisasola, J.A. Baeza, J. Carrera, G. Sin, P.A. Vanrolleghem, J. Lafuente, The influence of experimental data quality and quantity on parameter estimation accuracy, Educ. Chem. Eng. 1 (1) (2006) 139–145, https://doi.org/10.1205/ece06016.
[35] D. Wallach, Evaluating crop models. Work. with Dyn. Crop Model. Eval. Anal. Parameterization, Appl, Elsevier, 2006, pp. 11–54. https://www.elsevier.com/books/working-with-dynamic-crop-models/wallach/978-0-444-52135-4.
[36] A. Ribera-Guardia, M. Pijuan, Distinctive NO and N2O emission patterns in ammonia oxidizing bacteria: Effect of ammonia oxidation rate, DO and pH, Chem. Eng. J. 321 (2017) 358–365, https://doi.org/10.1016/j.cej.2017.03.122.
[37] V.C. Machado, J. Lafuente, J.A. Baeza, Activated sludge model 2d calibration with full-scale WWTP data: comparing model parameter identifiability with influent and operational uncertainty, Bioprocess Biosyst. Eng. 37 (7) (2014) 1271–1287, https://doi.org/10.1007/s00449-013-1099-8.
[38] G. Tallec, J. Garnier, G. Billen, M. Gousailles, Nitrous oxide emissions from secondary activated sludge in nitrifying conditions of urban wastewater treatment plants: Effect of oxygenation level, Water Res. 40 (15) (2006) 2972–2980, https://doi.org/10.1016/j.watres.2006.05.037.